Nuclear Polarization by Intense Laser Pulses

Hanxu Zhang,[1,2,3] Tao Li,[1] and Xu Wang[1,*]
[1]Graduate School, China Academy of Engineering Physics, Beijing 100193, China
[2]Key Laboratory of Nuclear Physics and Ion-beam Application (MOE), Institute of Modern Physics, Fudan University, Shanghai 200433, China
[3]Shanghai Research Center for Theoretical Nuclear Physics, NSFC and Fudan University, Shanghai 200438, China

(Received 7 November 2025; revised 14 April 2026; accepted 9 September 2026; published 5 October 2026)

Nuclear polarization plays an essential role in precision measurements, symmetry tests, and emerging quantum technologies, yet efficient polarization of heavy nuclei remains a major challenge. We propose an efficient, intense-laser-based approach that achieves high-efficiency polarization of heavy nuclei through the nonlinear interaction of circularly polarized femtosecond laser pulses with hydrogenlike ions. This scheme enables rapid transfer of angular momentum from light to the nucleus. Numerical simulations show that a single pulse can generate polarization exceeding 10%, while a pulse sequence can drive the system to near-unity polarization. The method is broadly applicable to heavy ions with large hyperfine splittings, as demonstrated for ^{229}Th, ^{205}Pb, and ^{209}Bi. The ability to produce near-complete polarization of large-spin nuclei and heavy ions opens new avenues for nuclear physics and nucleus-based quantum technologies.

DOI: 10.1103/p7k8-mjn7

Introduction—The polarization of atomic nuclei is a powerful tool for both fundamental research and technological applications. Polarized nuclei serve as sensitive probes for precision studies of nuclear forces and spin-dependent interactions [1–4], as well as for stringent tests of fundamental symmetries and searches for possible temporal or spatial variations of physical constants [5–13]. Beyond fundamental physics, nuclear polarization underpins enhanced nuclear magnetic resonance (NMR) sensitivity, improved magnetic resonance imaging (MRI) contrast, dynamic nuclear polarization in chemistry and biology [14,15], and emerging quantum information applications based on nuclear spins [16–18].

Established polarization techniques—including dynamic nuclear polarization [19–24], optical pumping [25–31], and spin-exchange collisions [32–36]—have achieved remarkable success. These approaches typically rely on resonant light-atom coupling driven by relatively weak laser fields, and consequently require species-specific laser frequencies to satisfy resonance conditions. Besides, these approaches have been mostly applied to relatively light nuclei. The goal of the current Letter is to propose a complementary, intense-laser-based approach for efficient polarization of heavy nuclei. Our scheme exploits qualitatively distinct features of strong-field light-matter interaction. First, transitions can proceed efficiently even under nonresonant conditions, alleviating the need for precise frequency matching. Second, the interaction occurs on ultrashort timescales (typically 10–100 fs), enabling rapid and coherent control. Intense laser-matter interactions have been widely used to generate attosecond pulses [37,38], to control ultrafast electronic dynamics [39–41], and to accelerate particles via laser-plasma interactions [42,43]. More recently, the possibility of using intense lasers to excite or manipulate nuclear states has emerged as a frontier direction [44–49]. Nevertheless, the use of intense laser pulses for nuclear polarization has, to our knowledge, remained largely unexplored.

Specifically, we investigate the interaction between intense circularly polarized (CP) laser pulses and nuclei embedded in hydrogenlike ions, as illustrated in Fig. 1. Unlike bare nuclei—whose extremely weak transition moments make direct optical polarization virtually

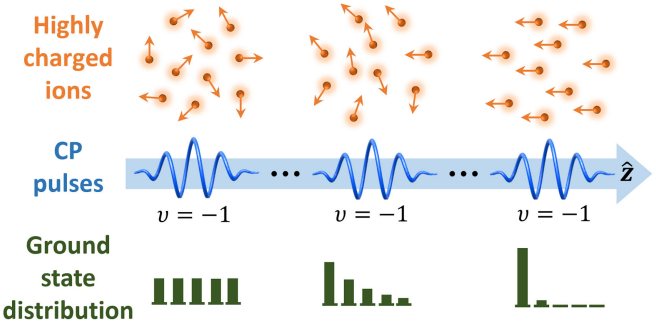


FIG. 1. Schematic illustration of the proposed approach. A sequence of circularly polarized laser pulses (e.g., with helicity $\nu = -1$) propagating along the z axis induces a directional transfer of population among magnetic sublevels of hydrogenlike ions, driving an initially unpolarized ensemble toward a polarized edge state.

*Contact author: xwang@gscaep.ac.cn

 © 2026 American Physical Society

impossible—hydrogenlike ions possess a bound $1s$ electron that mediates strong coupling between the laser field and the nucleus. Numerical simulations show that a single CP pulse can induce nuclear polarization exceeding 10% (the definition of polarization degree will be given below), while a pulse sequence can drive the system toward near-unity polarization. The proposed mechanism is broadly applicable to highly charged heavy ions with hyperfine splittings on the order of 1 eV. Representative examples include low-radioactivity nuclei such as ^{229}Th, ^{205}Pb, and ^{209}Bi.

Energy structure of hydrogenlike ions—The spin and parity of the nuclear ground state of ^{229}Th, ^{205}Pb, and ^{209}Bi are $5/2^+$, $5/2^-$, and $9/2^-$, respectively. In addition, ^{229}Th possesses a low-lying (8.4 eV) isomeric state with spin and parity $3/2^+$ [50–52]. Other nuclear states are irrelevant for the current Letter because they are too high to be populated. These nuclei are weakly radioactive: ^{229}Th undergoes α decay with a half-life of 7920 years [9], ^{205}Pb decays via electron capture with a half-life of 1.7×10^7 years [53], and ^{209}Bi undergoes α decay with a half-life of 2×10^{19} years [54].

For a hydrogenlike ion, the $1s$ electron with angular momentum $J = 1/2$ couples with the nucleus, splitting each nuclear state into two hyperfine states with total angular momentum $F = I \pm 1/2$ (I being the spin of the nuclear state). The system is described by the Hamiltonian $H_0 = H_\mathrm{n} + H_\mathrm{e} + V_\mathrm{HF}$, where H_n and H_e are the nuclear and the electronic Hamiltonians, respectively, and $V_\mathrm{HF} = \sum_{\tau\lambda\mu}(-1)^\mu \mathcal{M}^{(\tau\lambda-\mu)} \cdot \mathcal{N}^{(\tau\lambda\mu)}$ is the hyperfine interaction, with $\mathcal{M}^{(\tau\lambda)}$ and $\mathcal{N}^{(\tau\lambda)}$ being type-τ (E for electric, M for magnetic) and rank-λ tensor operators acting in the nuclear and the electronic subspaces, respectively. μ is the magnetic quantum number corresponding to λ. Detailed expressions of the tensor operators can be found in Refs. [55,56]. The eigenstate of the nucleus-electron system (i.e., the hyperfine state) can be written as

$$|F_i, m_i\rangle = \sum_{m_I, m_J} C^{F_i, m_i}_{J, m_J, I, m_I} |J, m_J\rangle |I, m_I\rangle, \tag{1}$$

TABLE I. Hyperfine structures and properties of hydrogenlike ions ^{229}Th^{89+}, ^{205}Pb^{81+}, and ^{209}Bi^{82+}.

	$\mu_I(\mu_\mathrm{N})$	I	Eigenstate	Energy (eV)	$T_{1/2}$ (ms)
^{229}Th^{89+}	−0.37	3/2	$\lvert F_4 = 1\rangle$	9.302	21.48
			$\lvert F_3 = 2\rangle_+$	8.484	20.52
	0.36	5/2	$\lvert F_2 = 3\rangle$	0.731	107.52
			$\lvert F_1 = 2\rangle_+$	0	
^{205}Pb^{81+}	0.71	5/2	$\lvert F_2 = 3\rangle$	0.922	49.9
			$\lvert F_1 = 2\rangle$	0	
^{209}Bi^{82+}	4.11	9/2	$\lvert F_2 = 5\rangle$	5.206	0.26
			$\lvert F_1 = 4\rangle$	0	

where $C^{F_i, m_i}_{J, m_J, I, m_I}$ is a Clebsch-Gordan coefficient, and m_i, m_J, and m_I are the magnetic quantum numbers of F_i, J, and I, respectively.

Table I lists the hyperfine structures and properties of the three hydrogenlike ions. For ^{229}Th^{89+}, the nuclear ground state splits into $F = 2$ and 3, while the isomeric state splits into $F = 2$ and 1. The subscripts in $|F_1 = 2\rangle_+$ and $|F_3 = 2\rangle_+$ indicate a nuclear hyperfine mixing (NHM) effect, which allows mixing between the two states with total angular momentum $F = 2$. The NHM effect modifies the energy levels and especially the radiative lifetime of the isomeric state [57–61]. For ^{205}Pb^{81+} and ^{209}Bi^{82+}, NHM is absent. The nuclear ground state of ^{205}Pb splits into two levels with $F = 2$ and 3. The nuclear ground state of ^{209}Bi splits into two levels with $F = 4$ and 5 with a relatively large splitting energy of 5.2 eV, due to the larger nuclear spin and magnetic moment. For simplicity in notation, in the following we label all the hyperfine sublevels by a single index $|n\rangle$ with $n = 1, \ldots, N$, where $N = \sum_i (2F_i + 1)$ is the total number of states in the system.

The half-lives of the excited hyperfine states are determined by the magnetic dipole ($M1$) transition rates, with $T_{1/2} = \ln 2/\Gamma$. For a transition from state n to state m, the transition rate is

$$\Gamma^{(M1)}_{n\to m} = \frac{4}{3} k^3_{nm} \left| \sum\nolimits_\mu \langle m | \mathcal{M}^{(M1\mu)} + \mathcal{T}^{(M1\mu)} | n \rangle \right|^2, \tag{2}$$

where $k_{nm} = k_n - k_m$ is the wave number corresponding to the transition energy. Here,

$$\mathcal{T}^{(M1\mu)} = -\frac{i}{c}\sqrt{\frac{\pi}{3}} \int \boldsymbol{j}_\mathrm{e} \cdot \boldsymbol{L}[r Y_{1\mu}(\theta, \phi)] d\tau \tag{3}$$

is the electronic magnetic moment operator, with $\boldsymbol{j}_\mathrm{e}$ and $\boldsymbol{L}$ denoting the electronic current density operator and angular momentum operator, respectively, and $Y_{1\mu}$ the spherical harmonics. The last column of Table I presents the half-lives of the excited states after averaging over initial states and summing over final states. The half-lives range from approximately 0.1 to 100 ms.

Nuclear polarization by intense laser pulses—The proposed approach proceeds through an excitation-decay cycle. Initially, the ions are uniformly distributed among the ground states $|F_1, m_1\rangle$, with equal probability for each magnetic substate. A CP femtosecond laser pulse drives strong oscillations between the hyperfine ground and the excited states, transferring angular momentum from the field to the system and creating an imbalance among the magnetic substates. After the pulse, the excited states relax back to the ground states within 0.1–100 ms via spontaneous photon emission, preserving the laser-induced population bias and thus generating nuclear polarization. The resulting polarized ground-state distribution serves as

the initial condition for the next pulse, which further amplifies the degree of polarization.

During the excitation stage, the dynamics of the system is governed by a time-dependent Dirac equation (TDDE),

$$i\hbar\frac{\partial}{\partial t}|\Psi(t)\rangle = [H_0 + H_{\rm I}(t)]|\Psi(t)\rangle, \tag{4}$$

where the interaction Hamiltonian with the laser field is

$$H_{\rm I}(t) = -\frac{1}{c}\int [\boldsymbol{j}_{\rm n}(\boldsymbol{r}) + \boldsymbol{j}_{\rm e}(\boldsymbol{r})]\cdot \boldsymbol{A}(\boldsymbol{r},t)d\tau, \tag{5}$$

with $\boldsymbol{j}_{\rm n}$ and $\boldsymbol{j}_{\rm e}$ the nuclear and electronic current density operators, respectively, c the speed of light, and $\boldsymbol{A}(\boldsymbol{r},t)$ the laser vector potential. We take the laser to propagate along $\hat{z}$ with right-handed circular polarization, and the polarization vector is $\boldsymbol{\epsilon} = \hat{e}_{-1} = (\hat{x} - i\hat{y})/\sqrt{2}$.

Expanding the wave function with the eigenstates of H_0: $|\Psi(t)\rangle = \sum_n C_n(t)e^{-i\omega_n t}|n\rangle$, the TDDE changes into a coupled set of ordinary differential equations for the expansion coefficients: $i\hbar\dot{C}_m(t) = \sum_n H_{\rm I}^{mn}(t)e^{i\omega_{mn}t}C_n(t)$. Here the interaction matrix element $H_{\rm I}^{mn}(t) = \langle m|H_{\rm I}(t)|n\rangle$ and $\omega_{mn} = \omega_m - \omega_n$. This set of equations can be numerically solved to obtain the time evolution of the amplitudes $C_n(t)$, from which the distribution across all hyperfine states at the end of the laser pulse t_f is given by $|C_n(t_f)|^2$.

The angular momentum transfer from the laser to the system can be understood from the structure of the interaction matrix elements. For CP lasers, the matrix element is $H_{\rm I}^{mn}e^{i\omega_{mn}t} \propto E_{\rm I}\mathcal{F}(t)$, where $E_{\rm I}$ is the interaction energy and $\mathcal{F}(t)$ takes the form

$$f_{mn}^{-}(t)\begin{pmatrix} F_m & 1 & F_n \\ -m_m & \nu & m_n \end{pmatrix} + f_{mn}^{+}(t)\begin{pmatrix} F_m & 1 & F_n \\ -m_m & -\nu & m_n \end{pmatrix}, \tag{6}$$

where $f_{mn}^{\pm}(t) = e^{i(\omega_{mn}\pm\omega_l)t}$. For excitation ($\omega_{mn} > 0$), $f_{mn}^{-}(t)$ is a corotating term and the $m_n + \nu$ channel is favored, while for de-excitation ($\omega_{nm} = -\omega_{mn} < 0$), $f_{nm}^{+}(t)$ is corotating and the $m_m - \nu$ channel is favored. This dynamical asymmetry leads to an imbalance in the population transfer among magnetic sublevels. Details of the derivation for both CP and linearly polarized (LP) lasers are given in Supplemental Material (SM) [62].

After the laser pulse, spontaneous decay begins. The population $|C_n(t_f)|^2$ in an excited substate $|n\rangle$ decays into ground substates $|F_1, m_1\rangle$ according to the $M1$ transition rates given by Eq. (2). Once relaxation is complete, all population resides in the ground manifold, and the degree of polarization is defined as

$$\mathcal{P} = \left|\frac{\sum_{m_1} p_{m_1} m_1}{F_1}\right|, \tag{7}$$

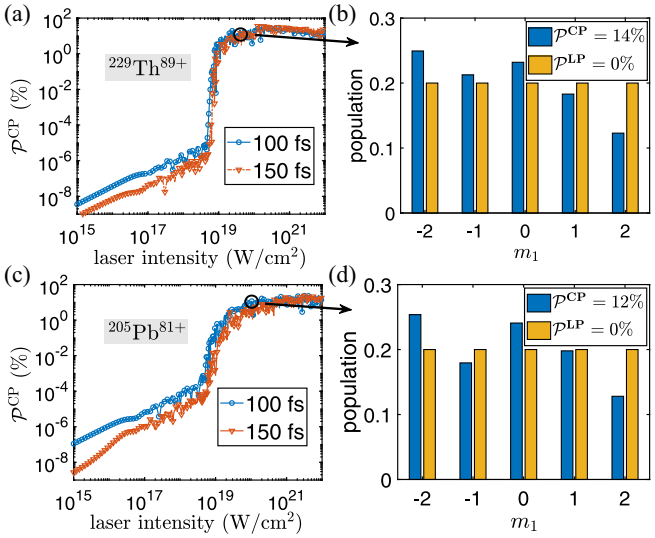


FIG. 2. Degree of polarization of ^{229}Th^{89+} and ^{205}Pb^{81+} after a single excitation-decay cycle at a laser wavelength of 1053 nm for circular polarization. (a),(c) Polarization degree as a function of laser intensity and pulse duration. (b) Ground state population distribution of ^{229}Th^{89+} after one excitation-decay cycle. CP and LP laser pulses are used with intensity 4×10^{19} W/cm^2 and pulse duration 150 fs. (d) Ground state population distribution of ^{205}Pb^{81+} after one excitation-decay cycle. CP and LP laser pulses are used with intensity 10^{20} W/cm^2 and pulse duration 100 fs.

where p_{m_1} is the probability of occupying substate $|F_1, m_1\rangle$.

This completes one excitation-decay cycle. The resulting partially polarized ground-state distribution then becomes the initial condition for the next laser pulse, which further enhances the polarization. An illustration of the polarization cycle and population evolution is given in SM [62].

Numerical results—We first examine the polarization of ^{229}Th^{89+} and ^{205}Pb^{81+} following interaction with a single CP pulse of wavelength 1053 nm and duration 100 fs and 150 fs, respectively. Figures 2(a) and 2(c) display the resulting degree of polarization (noted as $\mathcal{P}^{\rm CP}$) after one excitation-decay cycle. Below 10^{19} W/cm^2, $\mathcal{P}^{\rm CP}$ increases with the intensity but remains very small. A sharp increase occurs around 10^{19} W/cm^2, where a modest rise in intensity yields a 6–7 order-of-magnitude enhancement in polarization. This is due to the onset of a highly nonlinear interaction regime, where the interaction energy $E_{\rm I}$ becomes comparable to the transition energy (~1 eV) at 10^{19} W/cm^2, enabling efficient transfer of energy and angular momentum to the ions [63–67]. Around 10^{20} W/cm^2, the degree of polarization reaches the 10% level, demonstrating very efficient nuclear polarization induced by a single femtosecond laser pulse.

Figure 2(b) shows the population distribution of ^{229}Th^{89+} among the ground substates after one excitation-decay cycle, for CP and LP pulses with intensity

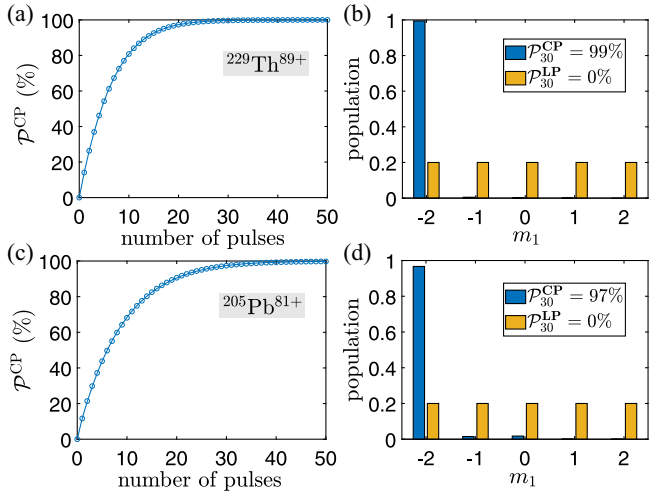


FIG. 3. (a) Degree of polarization of ^{229}Th^{89+} versus number of CP pulses. (b) Ground state population distribution of ^{229}Th^{89+} after 30 CP or LP pulses. (c) Degree of polarization of ^{205}Pb^{81+} versus number of CP pulses. (d) Ground state population distribution of ^{205}Pb^{81+} after 30 CP or LP pulses. Pulse parameters in (a),(b) are the same as in Fig. 2(b), and those in (c), (d) are the same as in Fig. 2(d).

4×10^{19} W/cm^2 and pulse duration 150 fs. For the LP pulse, the distribution remains uniform, yielding no polarization. In contrast, CP driving favors substates with lower m_1 owing to the choice of polarization vector $\hat{e}_{-1}$ (higher m_1 substates would be favored if the polarization vector were chosen to be $\hat{e}_{+1}$), giving $\mathcal{P}^{\rm CP} = 14\%$. A similar trend is found for ^{205}Pb^{81+} [Fig. 2(d)], where a 100 fs pulse at 10^{20} W/cm^2 yields $\mathcal{P}^{\rm CP} = 12\%$. While Figs. 2(a) and 2(c) show cases with even higher performance, reaching maximal degrees of polarization exceeding 40%, we highlight these two examples to illustrate the robustness of the method over a broad range of laser parameters. The difference between ^{229}Th^{89+} and ^{205}Pb^{81+} stems from their distinct energy structures, yet both exhibit comparable degrees of polarization with currently accessible laser intensities.

Near-complete polarization can be achieved through consecutive interactions with multiple pulses. For laser intensities around 10^{20} W/cm^2, typical repetition rates of 1–10 Hz [68–71] allow the system to decay to the ground state before the arrival of the next pulse. Figure 3(a) shows the polarization degree of ^{229}Th^{89+} as a function of pulse number, using the same CP pulses as in Fig. 2(b). The polarization increases monotonically, reaching nearly 100% after a few tens of pulses. The corresponding distribution [Fig. 3(b)] shows almost all population concentrated in the edge state $m_1 = -2$. In contrast, repeated LP pulses produce no polarization. Figures 3(c) and 3(d) present the results for ^{205}Pb^{81+}, where 30 CP pulses yield 97% polarization, approaching 100% with additional pulses.

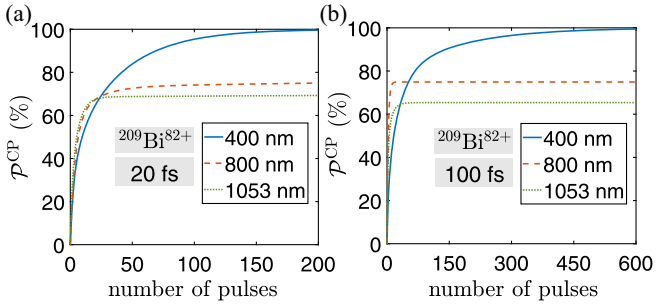


FIG. 4. Degree of polarization of ^{209}Bi^{82+} as a function of the number of CP pulses. Three different laser wavelengths are used with the same peak intensity of 10^{21} W/cm^2. (a) Pulse duration 20 fs. (b) Pulse duration 100 fs.

Figure 4 shows the polarization degree of ^{209}Bi^{82+} as a function of pulse numbers for three laser wavelengths and two pulse durations. In contrast to ^{229}Th^{89+} and ^{205}Pb^{81+}, which have hyperfine splittings below 1 eV, ^{209}Bi^{82+} has a much larger splitting of 5.2 eV (see Table I). This makes it more challenging to drive population transfer from the ground to the excited states. Our results show that shorter wavelengths, such as 400 nm, are more efficient than 800 or 1053 nm at the same intensity.

For short pulses of 20 fs [Fig. 4(a)], all three wavelengths achieve polarization above 70%, with 400 nm performing best and reaching 100% after about 200 pulses. For longer 100-fs pulses [Fig. 4(b)], the 400-nm case again outperforms the others, achieving full polarization after ~500 pulses. Interestingly, 800 nm and 1053 nm can induce relatively higher polarization at early stages with fewer pulses, suggesting that judicious combinations of pulse parameters—such as long 800-nm pulses followed by short 400-nm pulses—could further enhance the polarization efficiency.

Discussions—First, the polarization degree of a hydrogenlike ion is directly related to that of the bare nucleus. For instance, the fully polarized state of ^{205}Pb^{81+} is

$$\begin{aligned}|F_1 = 2, m_1 = -2\rangle &= \sqrt{\frac{5}{6}}\left|J = \frac{1}{2}, m_J = \frac{1}{2}\right\rangle\left|I = \frac{5}{2}, m_I = -\frac{5}{2}\right\rangle \\ &\quad - \sqrt{\frac{1}{6}}\left|J = \frac{1}{2}, m_J = -\frac{1}{2}\right\rangle\left|I = \frac{5}{2}, m_I = -\frac{3}{2}\right\rangle, \quad (8)\end{aligned}$$

which is a superposition of electron and nuclear spin states. By applying Eq. (7) with F_1 and m_1 replaced by I and m_I, the resulting nuclear polarization is 93.33%. Likewise, a fully polarized ^{209}Bi^{82+} ion corresponds to 97.78% nuclear polarization.

Note that a polarized hydrogenlike ion is already an ideal platform for studying nuclear polarization, offering clean systems for precision spectroscopy, spin-dependent

interaction studies, and fundamental tests in extreme electromagnetic fields [72–74]. Stripping off the remaining electron is not needed.

Second, the proposed polarization scheme exploits the interaction of hydrogenlike ions with intense laser fields, driving nonlinear population oscillations between hyperfine levels separated by about 1 eV. The bound $1s$ electron plays a crucial role, both by enhancing coupling to the laser field and by generating the hyperfine structure that enables efficient angular-momentum transfer. In contrast, bare nuclei lack this bridge—their minute nuclear transition moments make direct laser coupling negligibly weak. Indeed, calculations including only the nuclear ground substates show virtually no polarization, even at intensities as high as 10^{23} W/cm^2, the current experimental limit [70].

Third, our approach can be viewed as a strong-field version of optical pumping. Conventional optical pumping transfers angular momentum via resonant absorption and spontaneous emission cycles, building polarization gradually over micro- to millisecond timescales. In contrast, our approach retains the same physical principle—angular-momentum transfer from CP photons—but extends it into the nonresonant, highly nonlinear regime accessible with today's intense lasers. Previous studies on laser-induced spin dynamics mainly focus on condensed-matter systems with much lower intensities ($< 10^{12}$ W/cm^2), where the laser acts as a heating source that drives nonequilibrium spin dynamics and relaxation [75–79]. Our approach targets highly charged heavy ions confined in ion traps, where strong-field driving enables polarization without relying on resonance or detailed knowledge of nuclear level structures. This method is therefore particularly suited to few-ion precision measurements, where the same ions can be repeatedly addressed in a low-density environment. By contrast, its applicability to large-scale polarization production involving light nuclei and condensed systems is limited, as strong-field ionization and plasma effects may become dominant in such regimes.

Fourth, this approach exhibits robustness in several important aspects. (i) It does not rely on resonance: the 400, 800, and 1053 nm pulses used here (3.10, 1.55, and 1.17 eV photons) are far off-resonant with any hyperfine gap, yet still achieve efficient polarization; (ii) despite differences in nuclear energy levels, spins, and magnetic dipole moments, efficient polarization can be realized across nuclei. The three nuclei studied here, with distinct energy structures, illustrate the generality of the method; (iii) for hydrogenlike ions, the $1s$ electron is highly stable, with excitation energies to the $2p$ orbital on the order of 10 keV, ensuring that the electron remains in the ground state throughout the laser interaction; (iv) non-$M1$ channels during the excitation-decay cycle can be neglected due to the much smaller nuclear multipole moments compared with the electronic magnetic dipole moment. For instance, $E2$ transitions are extremely weak, with a characteristic scale $Q_0/\mu_e \sim 10^{-10}$ (Q_0 being the nuclear electric quadrupole moment on the order of $e \cdot$ barn), while higher-order multipoles are expected to be even smaller. In addition, the method remains effective for initially nonuniform sublevel distributions, as demonstrated in SM [62].

Fifth, our approach is experimentally feasible with existing facilities [71,80–91]. Hydrogenlike ions can be produced using accelerators or electron beam ion traps (EBITs) [92–94] and subsequently confined in ion storage rings or cryogenic Penning traps, where long trapping times (up to days), low temperatures (4–10 K), and ion densities up to 10^9 cm^{-3} can be achieved [84,86,90]. Rethermalization among different magnetic sublevels is expected to be negligible over the timescale of multiple pulses, as to be discussed below. Intense laser systems with intensities of 10^{20}–10^{21} W/cm^2 have already been integrated with Penning traps [71,84–88].

With Penning trap platforms, possible perturbations are minimal. (a) The spatial overlap between the ion ensemble and the laser focus can be adjusted by the ion number and beam waist. The ion motion induced during the femtosecond laser pulse ($\lesssim 1$ μm) is negligible compared to the focal size, and the residual heating after the pulse is small and can be efficiently removed by standard resistive cooling techniques [95–97]. The residual ion motion induced by the ponderomotive force can be mitigated by adjusting the laser intensity, pulse duration, beam waist, and repetition rate. (b) Because of the nonresonant nature of our approach, Doppler effects do not affect the polarization process. (c) Magnetic fields in Penning traps ($B \sim 7$ T, $\Delta B \sim 1$ nT) induce Zeeman splittings ($\sim 10^{-3}$ eV) much smaller than the hyperfine structure and therefore do not affect the dynamics considered here. (d) Depolarization effects are also strongly suppressed: ion-ion collisions are insufficient to induce internal transitions due to the low temperature, and blackbody-radiation-induced relaxation between magnetic sublevels occurs on timescales of decades. More detailed estimates are given in SM [62].

Conclusion—We have proposed a new scheme for nuclear polarization based on intense laser interactions with hydrogenlike ions. A single femtosecond pulse can generate polarization on the order of 10%, while a sequence of pulses enables near 100% polarization. The high efficiency stems from the large magnetic dipole moment of the $1s$ electron, which strengthens laser-nucleus coupling and opens magnetic-dipole transition channels through hyperfine interactions. The method is broadly applicable, as illustrated with ^{229}Th, ^{205}Pb, and ^{209}Bi, which span a wide range of nuclear spins, energy structures, and hyperfine splittings. Our results show that presently available intense lasers can enable strong nuclear and heavy ion polarization, providing a practical route toward efficient nuclear spin control with potential applications in quantum information, precision spectroscopy, and fundamental nuclear physics.

Acknowledgments—We acknowledge helpful discussions with Professor Bingsheng Tu from Fudan University. This work was supported by NSFC Grants No. 12474484, No. U2330401, No. 12088101, and No. 12547102.

Data availability—The data that support the findings of this Letter are openly available [98].

[1] M. E. Rose, On the production of nuclear polarization, Phys. Rev. **75**, 213 (1949).

[2] R. V. Pound, On the spatial alignment of nuclei, Phys. Rev. **76**, 1410 (1949).

[3] L. Cong, W. Ji, P. Fadeev, F. Ficek, M. Jiang, V. V. Flambaum, H. Guan, D. F. Jackson Kimball, M. G. Kozlov, Y. V. Stadnik, and D. Budker, Spin-dependent exotic interactions, Rev. Mod. Phys. **97**, 025005 (2025).

[4] A. Yachmenev and G. Yang, Nuclear spin symmetry breaking and spin polarization in rotational energy level clusters, Phys. Rev. Res. **7**, L032047 (2025).

[5] P. Yu and N. R. Hutzler, Probing fundamental symmetries of deformed nuclei in symmetric top molecules, Phys. Rev. Lett. **126**, 023003 (2021).

[6] V. V. Flambaum, Enhanced effect of temporal variation of the fine structure constant and the strong interaction in ^{229}Th, Phys. Rev. Lett. **97**, 092502 (2006).

[7] H. Li, L. G. Pang, Q. Wang, and X. L. Xia, Global Λ polarization in heavy-ion collisions from a transport model, Phys. Rev. C **96**, 054908 (2017).

[8] P. Fadeev, J. C. Berengut, and V. V. Flambaum, Sensitivity of ^{229}Th nuclear clock transition to variation of the fine-structure constant, Phys. Rev. A **102**, 052833 (2020).

[9] K. Beeks, T. Sikorsky, T. Schumm, J. Thielking, M. V. Okhapkin, and E. Peik, The thorium-229 low-energy isomer and the nuclear clock, Nat. Rev. Phys. **3**, 238 (2021).

[10] STAR Collaboration, Pattern of global spin alignment of ϕ and K^{*0} mesons in heavy-ion collisions, Nature (London) **614**, 244 (2023).

[11] L. Y. Wu, K. Y. Zhang, M. Peng, J. Gong, and H. Yan, New limits on exotic spin-dependent interactions at astronomical distances, Phys. Rev. Lett. **131**, 091002 (2023).

[12] T. Niida and S. A. Voloshin, Polarization phenomenon in heavy-ion collisions, Int. J. Mod. Phys. E **33**, 2430010 (2024).

[13] K. Zhang, L. Wu, and H. Yan, New limits on ultralight axionlike dark matter from reanalyzed data, Phys. Rev. Lett. **135**, 131001 (2025).

[14] T. Biedenbänder, V. Aladin, S. Saeidpour, and B. Corzilius, Dynamic nuclear polarization for sensitivity enhancement in biomolecular solid-state NMR, Chem. Rev. **122**, 9738 (2022).

[15] S. Jannin, J. N. Dumez, P. Giraudeau, and D. Kurzbach, Application and methodology of dissolution dynamic nuclear polarization in physical, chemical and biological contexts, J. Magn. Reson. **305**, 41 (2019).

[16] A. A. Wood, R. M. Goldblatt, R. E. Scholten, and A. M. Martin, Quantum control of nuclear-spin qubits in a rapidly rotating diamond, Phys. Rev. Res. **3**, 043174 (2021).

[17] X. Gao, S. Vaidya, K. Li, P. Ju, B. Jiang, Z. Xu, A. E. L. Allcca, K. Shen, T. Taniguchi, K. Watanabe *et al.*, Nuclear spin polarization and control in hexagonal boron nitride, Nat. Mater. **21**, 1024 (2022).

[18] F. Becattini, Spin and polarization: A new direction in relativistic heavy ion physics, Rep. Prog. Phys. **85**, 122301 (2022).

[19] A. W. Overhauser, Polarization of nuclei in metals, Phys. Rev. **92**, 411 (1953).

[20] A. W. Overhauser, Paramagnetic relaxation in metals, Phys. Rev. **89**, 689 (1953).

[21] T. R. Carver and C. P Slichter, Polarization of nuclear spins in metals, Phys. Rev. **92**, 212 (1953).

[22] M. Abraham, M. A. H. McCausland, and F. N. H. Robinson. Dynamic nuclear polarization, Phys. Rev. Lett. **2**, 449 (1959).

[23] A. Abragam and M. Goldman, Principles of dynamic nuclear polarisation, Rep. Prog. Phys. **41**, 395 (1978).

[24] T. Maly, G. T. Debelouchina, V. S. Bajaj, K. Hu, C. Joo, M. L. Mak–Jurkauskas, J. R. Sirigiri, P. C. A. van der Wel, J. Herzfeld, R. J. Temkin, and R. G. Griffin, Dynamic nuclear polarization at high magnetic fields, J. Chem. Phys. **128**, 052211 (2008).

[25] C. Cohen-Tannoudji and A. Kastler, *I Optical Pumping in Progress in Optics* (Elsevier, Amsterdam, 1966), Vol. 5.

[26] F. D. Colegrove, L. D. Sghearer, and G. K. Walters, Polarization of He^3 gas by optical pumping, Phys. Rev. **132**, 2561 (1963).

[27] D. S. Hussey, D. R. Rich, A. S. Belov, X. Tong, H. Yang, C. Bailey, C. D. Keith, J. Hart, G. D. R. Hall, T. C. Black *et al.*, Polarized ^{3}He gas compression system using metastability-exchange optical pumping, Rev. Sci. Instrum. **76**, 053503 (2005).

[28] A. Nikiel, T. Palasz, M. Suchanek, M. Abboud, A. Sinatra, Z. Olejniczak, T. Dohnalik, G. Tastevin, and P-J. Nacher, Metastability exchange optical pumping of ^{3}He at high pressure and high magnetic field for medical applications, Eur. Phys. J. Special Topics **144**, 255 (2007).

[29] M. Abboud, A. Sinatra, X. Maître, G. Tastevin, and P. J. Nacher, High nuclear polarization of ^{3}He at low and high pressure by metastability exchange optical pumping at 1.5 Tesla, Europhys. Lett. **68**, 480 (2004).

[30] M. Batz, P. J. Nacher, and G. Tastevin, Fundamentals of metastability exchange optical pumping in helium, J. Phys. Conf. Ser. **294**, 012002 (2011).

[31] Y. Wang, L. Wu, K. Zhang, M. Peng, S. Chen, and H. Yan, A polarized ^{3}He system based on metastability-exchange optical pumping, Sci. China Phys. Mech. Astron. **67**, 273011 (2024).

[32] B. Larson, O. Häusser, P. P. J. Delheij, D. M. Whittal, and D. Thiessen, Optical pumping of Rb in the presence of high-pressure ^{3}He buffer gas, Phys. Rev. A **44**, 3108 (1991).

[33] S. Appelt, A. B. Baranga, C. J. Erickson, M. V. Romalis, A. R. Young, and W. Happer, Theory of spin-exchange optical pumping of ^{3}He and ^{129}Xe, Phys. Rev. A **58**, 1412 (1998).

[34] E. Babcock, I. Nelson, S. Kadlecek, B. Driehuys, L. W. Anderson, F. W. Hersman, and T. G. Walker, Hybrid spin-exchange optical pumping of ^{3}He, Phys. Rev. Lett. **91**, 123003 (2003).

[35] T. G. Walker, Fundamentals of spin-exchange optical pumping, J. Phys. Conf. Ser. **294**, 012001 (2011).

[36] A. Korver, D. Thrasher, M. Bulatowicz, and T. G. Walker, Synchronous spin-exchange optical pumping, Phys. Rev. Lett. **115**, 253001 (2015).

[37] P. M. Paul, E. S. Toma, P. Breger, G. Mullot, F. Augé, Ph. Balcou, H. G. Muller, and P. Agostini, Observation of a train of attosecond pulses from high harmonic generation, Science **292**, 1689 (2001).

[38] M. Hentschel, R. Kienberger, Ch. Spielmann, G. A. Reider, N. Milosevic, T. Brabec, P. Corkum, U. Heinzmann, M. Drescher, and F. Krausz, Attosecond metrology, Nature (London) **414**, 509 (2001).

[39] A. Baltuška, Th. Udem, M. Uiberacker, M. Hentschel, E. Goulielmakis, Ch. Gohle, R. Holzwarth, V. S. Yakovlev, A. Scrinzi, T. W. Hänsch, and F. Krausz, Attosecond control of electronic processes by intense light fields, Nature (London) **421**, 611 (2003).

[40] M. Schultze, M. Fiess, N. Karpowicz, J. Gagnon, M. Korbman, M. Hofstetter, S. Neppl, A. L. Cavalieri, Y. Komninos, Th. Mercouris, C. A. Nicolaides *et al.*, Delay in photoemission, Science **328**, 1658 (2010).

[41] M. Nisoli, P. Decleva, F. Calegari, A. Palacios, and F. Martín, Attosecond electron dynamics in molecules, Chem. Rev. **117**, 10760 (2017).

[42] T. Tajima and J. M. Dawson, Laser electron accelerator, Phys. Rev. Lett. **43**, 267 (1979).

[43] M. Litos, E. Adli, W. An, C. I. Clarke, C. E. Clayton, S. Corde, J. P. Delahaye, R. J. England, A. S. Fisher, J. Frederico *et al.*, High-efficiency acceleration of an electron beam in a plasma wakefield accelerator, Nature (London) **515**, 7525 (2014).

[44] T. J. Bürvenich, J. Evers, and C. H. Keitel, Dynamic nuclear Stark shift in superintense laser fields, Phys. Rev. C **74**, 044601 (2006).

[45] Y. Wu, J. Gunst, C. H. Keitel, and A. Pálffy, Tailoring laser-generated plasmas for efficient nuclear excitation by electron capture, Phys. Rev. Lett. **120**, 052504 (2018).

[46] W. Wang, J. Zhou, B. Liu, and X. Wang, Exciting the isomeric ^{229}Th nuclear state via laser-driven electron recollision, Phys. Rev. Lett. **127**, 052501 (2021).

[47] C. Fu, G. Zhang, and Y. Ma, New opportunities for nuclear and atomic physics on the femto- to nanometer scale with ultra-high-intensity lasers, Matter Radiat. Extremes **7**, 024201 (2022).

[48] F. Negoita *et al.*, Laser driven nuclear physics at ELINP, arXiv:2201.01068.

[49] J. Feng *et al.*, Laser-based approach to measure small nuclear cross sections in plasma, Proc. Natl. Acad. Sci. U.S.A. **121**, e2413221121 (2024).

[50] J. Tiedau, M. V. Okhapkin, K. Zhang, J. Thielking, G. Zitzer, E. Peik, F. Schaden, T. Pronebner, I. Morawetz, L. T. De Col, F. Schneider, A. Leitner, M. Pressler, G. A. Kazakov, K. Beeks, T. Sikorsky, and T. Schumm, Laser excitation of the Th-229 nucleus, Phys. Rev. Lett. **132**, 182501 (2024).

[51] R. Elwell, C. Schneider, J. Jeet, J. E. S. Terhune, H. W. T. Morgan, A. N. Alexandrova, H. B. Tran Tan, A. Derevianko, and E. R. Hudson, Laser excitation of the ^{229}Th nuclear isomeric transition in a solid-state host, Phys. Rev. Lett. **133**, 013201 (2024).

[52] C. Zhang, T. Ooi, J. S. Higgins, J. F. Doyle, L. von der Wense, K. Beeks, A. Leitner, G. Kazakov, P. Li, P. G. Thirolf *et al.*, Frequency ratio of the ^{229m}Th nuclear isomeric transition and the ^{87}Sr atomic clock, Nature (London) **633**, 63 (2024).

[53] M. Wang, G. Audi, F. G. Kondev, W. Huang, S. Naimi, and X. Xu, The AME2016 atomic mass evaluation (II). Tables, graphs and references, Chin. Phys. C **41**, 030003 (2016).

[54] M. Wang, G. Audi, A. H. Wapstra, F. G. Kondev, M. MacCormick, X. Xu, and B. Pfeiffer, The AME2012 atomic mass evaluation, Chin. Phys. C **36**, 1603 (2012).

[55] C. Schwartz, Hyperfine structure, Phys. Rev. **97**, 380 (1955).

[56] K. Alder, A. Bohr, T. Huus, B. Mottelson, and A. Winther, Study of nuclear structure by electromagnetic excitation with accelerated ions, Rev. Mod. Phys. **28**, 432 (1956).

[57] S. Wycechand J. Żylicz, Predictions for nuclear spin mixing in magnetic fields. Acta Phys. Pol. B **24**, 637 (1993), https://www.actaphys.uj.edu.pl/fulltext?series=Reg&vol=24&page=637.

[58] F. F. Karpeshin, S. Wycech, I. M. Band, M. B. Trzhaskovskaya, M. Pfützner, and J. Żylicz, Rates of transitions between the hyperfine-splitting components of the ground-state and the 3.5 eV isomer in ^{229}Th^{89+}, Phys. Rev. C **57**, 3085 (1998).

[59] E. V. Tkalya and A. V. Nikolaev, Magnetic hyperfine structure of the ground-state doublet in highly charged ions ^{229}Th$^{89+,87+}$ and the Bohr-Weisskopf effect, Phys. Rev. C **94**, 014323 (2016).

[60] V. M. Shabaev, D. A. Glazov, A. M. Ryzhkov, C. Brandau, G. Plunien, W. Quint, A. M. Volchkova, and D. V. Zinenko, Ground-state g factor of highly charged ^{229}Th ions: An access to the M1 transition probability between the isomeric and ground nuclear states, Phys. Rev. Lett. **128**, 043001 (2022).

[61] W. Wang and X. Wang, Substantial nuclear hyperfine mixing effect in boronlike ^{205}Pb ions, Phys. Rev. Lett. **133**, 032501 (2024).

[62] See Supplemental Material at http://link.aps.org/supplemental/10.1103/p7k8-mjn7 for more detailed derivation of interaction matrix elements and discussion of experimental feasibility.

[63] H. Zhang, T. Li, and X. Wang, Highly nonlinear light-nucleus interaction, Phys. Rev. Lett. **133**, 152503 (2024).

[64] H. Zhang, T. Li, and X. Wang, Highly efficient nuclear excitation via highly nonlinear light-nucleus interaction, Phys. Rev. C **111**, 044614 (2025).

[65] J. Koch, G. R. Hunanyan, T. Ockenfels, E. Rico, E. Solano, and M. Weitz, Quantum Rabi dynamics of trapped atoms far in the deep strong coupling regime. Nat. Commun. **14**, 954 (2023).

[66] A. F. Kockum, A. Miranowicz, S. D. Liberato, S. Savasta, and F. Nori, Ultrastrong coupling between light and matter. Nat. Rev. Phys. **1**, 19 (2019).

[67] P. Forn-Díaz, L. Lamata, E. Rico, J. Kono, and E. Solano, Ultrastrong coupling regimes of light-matter interaction. Rev. Mod. Phys. **91**, 025005 (2019).

[68] D. L. Balabanski, R. Popescu, D. Stutman, K. A. Tanaka, O. Tesileanu, C. A. Ur, D. Ursescu, and N. V. Zamfir, New light

in nuclear physics: The extreme light infrastructure. Europhys. Lett. **117**, 28001 (2017).
[69] Z. Zhang, F. Wu, J. Hu, X. Yang, J. Gui, P. Ji, X. Liu, C. Wang, Y. Liu, X. Lu *et al.*, The 1 PW/0.1 Hz laser beamline in SULF facility, High Power Laser Sci. Eng. **8**, E4 (2020).
[70] J. W. Yoon, Y. G. Kim, I. W. Choi, J. H. Sung, H. W. Lee, S. K. Lee, and C. H. Nam, Realization of laser intensity over 10^{23} W/cm^2, Optica **8**, 630 (2021).
[71] Z. Major, U. Eisenbarth, B. Zielbauer, C. Brabetz, J. B. Ohland, Y. Zobus, S. Roeder, D. Reemts, S. Kunzer, S. Götte *et al.*, High-energy laser facility PHELIX at GSI: Latest advances and extended capabilities, High Power Laser Sci. Eng. **12**, e39 (2024).
[72] M. G. Kozlov, M. S. Safronova, J. R. Crespo López-Urrutia, and P. O. Schmidt, Highly charged ions: Optical clocks and applications in fundamental physics, Rev. Mod. Phys. **90**, 045005 (2018).
[73] J. Morgner, B. Tu, C, M. König, T. Sailer, F. Heiße, H. Bekker, B. Sikora, C. Lyu, V. A. Yerokhin, Z. Harman, J. R. Crespo López-Urrutia *et al.*, Stringent test of QED with hydrogen-like tin, Nature (London) **622**, 53 (2023).
[74] R. Loetzsch, H. F. Beyer, L. Duval, U. Spillmann, D. Banaś, P. Dergham, F. M. Kröger, J. Glorius, R. E. Grisenti, M. Guerra, A. Gumberidze *et al.*, Testing quantum electrodynamics in extreme fields using helium-like uranium, Nature (London) **625**, 673 (2024).
[75] J. He, S. Li, T. Frauenheim, and Z. Zhou, Ultrafast laser pulse induced transient ferrimagnetic state and spin relaxation dynamics in two-dimensional antiferromagnets, Nano Lett. **23**, 8348 (2023).
[76] S. Mankovsky, S. Polesya, and H. Ebert, Ultrafast spin dynamics: Role of laser-induced modification of exchange parameters, J. Phys. Condens. Matter **37**, 315801 (2025).
[77] A. Buzdakov, T. Blank, K. Zvezdin, O. Chubykalo-Fesenko, and A. Kimel, Modeling the diversity of laser-induced spin dynamics in Gd/Fe-Co multilayers, Phys. Rev. Appl. **23**, 044059 (2025).
[78] D. Pecchio, S. Sahoo, O. Chubykalo-Fesenko, S. Koraltan, G. M. Macauley, T. Thomson, D.Suess, V. Scagnoli, and L. J. Heyderman, Ultrafast laser-induced magnetic relaxation in artificial spin ice driven by dipolar interactions, Phys. Rev. B **113**, 064404 (2026).
[79] L. Du, Y. Lv, M. Duan, and A. Liu, Femtosecond laser-induced relaxation dynamics in ferromagnetic films, Discovery Phys. **2**, 4 (2026).
[80] L. S. Brown and G. Gabrielse, Geonium theory: Physics of a single electron or ion in a Penning trap, Rev. Mod. Phys. **58**, 233 (1986).
[81] S. W. Epp, J. R. Crespo López-Urrutia, G. Brenner, V. Mäckel, P. H. Mokler, R. Treusch, M. Kuhlmann, M. V. Yurkov, J. Feldhaus, J. R. Schneider, M. Wellhofer, M. Martins, W. Wurth, and J. Ullrich, Soft x-ray laser spectroscopy on trapped highly charged ions at FLASH, Phys. Rev. Lett. **98**, 183001 (2007).
[82] S. W. Epp, J. R. Crespo López-Urrutia, M. C. Simon, T. Baumann, G. Brenner, R. Ginzel, N. Guerassimova, V. Mäckel, P. H. Mokler, B. L. Schmitt, H. Tawara, and J. Ullrich, X-ray laser spectroscopy of highly charged ions at FLASH, J. Phys. B **43**, 194008 (2010).
[83] S. Bernitt, G. V. Brown, J. K. Rudolph, R. Steinbrügge, A. Graf, M. Leutenegger, S. W. Epp, S. Eberle, K. Kubiček, V. Mäckel *et al.*, An unexpectedly low oscillator strength as the origin of the Fe XVII emission problem, Nature (London) **492**, 225 (2012).
[84] M. Vogel, W. Quint, G. G. Paulus, and Th. Stöhlker, A Penning trap for advanced studies with particles in extreme laser fields, Nucl. Instrum. Methods Phys. Res., Sect. B **285**, 65 (2012).
[85] S. Sturm, I. Arapoglou, A. Egl, M. Höcker, S. Kraemer, T. Sailer, B. Tu, A. Weigel, R. Wolf, J. Crespo López-Urrutia *et al.*, The ALPHATRAP experiment, Eur. Phys. J. Special Topics **227**, 1425 (2019).
[86] S. Ringleb, M. Kiffer, N. Stallkamp, S. Kumar, J. Hofbrucker, B. Reich, B. Arndt, G. Brenner, M. Ruiz-Lopéz, S. Düsterer *et al.*, High-intensity laser experiments with highly charged ions in a Penning trap, Phys. Scr. **97**, 084002 (2022).
[87] B. A. Vining, G. Li, and A. G. Marshall, Laser-induced fluorescence for ion tomography in a Penning trap, J. Am. Soc. Mass Spectrom. **9**, 925 (1998).
[88] M. Vogel, G. Birkl, M. S. Ebrahimi, D. von Lindenfels, A. Martin, G. G. Paulus, W. Quint, S. Ringleb, Th. Stohlker, and M. Wiesel, Extreme-field physics in Penning traps The ARTEMIS and HILITE experiments, Hyperfine Interact. **236**, 65 (2015).
[89] D. A. Nesterenko, T. Eronen, A. Kankainen, L. Canete, A. Jokinen, I. D. Moore, H. Penttilä, S. Rinta-Antila, A. de Roubin, and M. Vilen, Phase-imaging ion-cyclotron-resonance technique at the JYFLTRAP double Penning trap mass spectrometer, Eur. Phys. J. A **54**, 154 (2018).
[90] J. Wang, J. Wu, T. Zhang, J. Liu, J. Peng, J. Wang, Y. Shen, B. Wei, Y. Zou, and B. Tu, Development and characteristics of a superconducting resonator and cryogenic low-noise amplifiers for Shanghai Penning trap, Nucl. Sci. Tech. **36**, 217 (2025).
[91] O. Kaleja, B. Anđelić, O. Bezrodnova, K. Blaum, M. Block, S. Chenmarev, P. Chhetri, C. Droese, Ch. E. Düllmann, M. Eibach, S. Eliseev *et al.*, Direct high-precision mass spectrometry of superheavy elements with SHIPTRAP, Phys. Rev. C **106**, 054325 (2022).
[92] R. E. Marrs, S. R. Elliott, and D. A. Knapp, Production and trapping of hydrogenlike and bare uranium ions in an electron beam ion trap, Phys. Rev. Lett. **72**, 4082 (1994).
[93] A. J. G. Martínez, J. C. López-Urrutia, D. Fischer, R. Soria Orts, and J. Ullrich, The Heidelberg EBIT: Present results and future perspectives. J. Phys. Conf. Ser. **72**, 012001 (2007).
[94] P. Micke, S. Kuhn, L. Buchauer, J. Harries, T. M. Bucking, K. Blaum, A. Cieluch, A. Egl, D. Hollain, S. Kraemer *et al.*, The Heidelberg compact electron beam ion traps. Rev. Sci. Instrum. **89**, 063109 (2018).
[95] M. Vogel, H. Häffner, K. Hermanspahn, S. Stahl, J. Steinmann, and W. Quint, Resistive and sympathetic cooling of highly-charged-ion clouds in a Penning trap, Phys. Rev. A **90**, 043412 (2014).

[96] M. S. Ebrahimi, Z. Guo, M. Vogel, M. Wiesel, G. Birkl, and W. Quint, Resistive cooling of highly charged ions in a Penning trap to a fluidlike state, Phys. Rev. A **98**, 023423 (2018).
[97] M. Kiffer, S. Ringleb, T. Stöhlker, and M. Vogel, Resistive cooling of ions' center-of-mass energy in a Penning trap on millisecond time scales, Phys. Rev. A **109**, 033012 (2024).
[98] H. Zhang, Nuclear polarization by intense laser pulses—figures, figshare, 10.6084/m9.figshare.33511525 (2026).